Fast-updating and nonrepeating Lissajous image reconstruction method for capturing increased dynamic information

Christopher L. Hoy,[1] Nicholas J. Durr,[2] and Adela Ben-Yakar[1,2,*]

[1]Department of Mechanical Engineering, The University of Texas at Austin, Austin, Texas 78712, USA

[2]Department of Biomedical Engineering, The University of Texas at Austin, Austin, Texas 78712, USA

*Corresponding author: ben-yakar@mail.utexas.edu

Received 29 November 2010; revised 7 February 2011; accepted 8 February 2011;
posted 8 February 2011 (Doc. ID 138842); published 23 May 2011

We present a fast-updating Lissajous image reconstruction methodology that uses an increased image frame rate beyond the pattern repeat rate generally used in conventional Lissajous image reconstruction methods. The fast display rate provides increased dynamic information and reduced motion blur, as compared to conventional Lissajous reconstruction, at the cost of single-frame pixel density. Importantly, this method does not discard any information from the conventional Lissajous image reconstruction, and frames from the complete Lissajous pattern can be displayed simultaneously. We present the theoretical background for this image reconstruction methodology along with images and video taken using the algorithm in a custom-built miniaturized multiphoton microscopy system. © 2011 Optical Society of America

OCIS codes: 100.3010, 100.2000, 180.5810.

1. Introduction

Lissajous scanning patterns are often employed in laser scanning systems where the more common raster scanning pattern is impractical. This is often the case in miniaturized laser scanning microscopes using microelectromechanical system (MEMS) scanning mirrors or piezoelectric fiber scanners for beam scanning [1–5]. In such devices, the frequency of the slow-axis deflection required for a raster scan is usually well below the mechanical resonance frequency. Actuation off resonance requires larger driving voltages, and the maximum achievable deflection angle is often much less than the maximum deflection achievable on resonance. In such cases, it becomes desirable to actuate both axes of the scanner at their mechanical resonance to achieve the maximum scanning angles and therefore the largest field of view (FOV). Scanning the laser with two orthogonal axes at resonance produces Lissajous scanning patterns [6].

In laser scanning microscopy applications, the frame rate of a Lissajous-scanned image is traditionally taken as the rate at which the Lissajous pattern repeats itself [2,3]. Selection of the driving frequencies determines the pattern repeat rate and requires optimization to maximize the imaging speed and the number of pixels in the image, while minimizing the number of unsampled pixels in a single frame.

Here we present a new implementation of Lissajous scanning and image reconstruction in which the imaging frame rate is significantly faster than the Lissajous pattern repeat rate to provide additional dynamic information. While we originally developed the technique for use in our miniaturized multiphoton imaging and femtosecond laser microsurgery probe [4], the technique is broadly applicable to any Lissajous-scanned laser scanning imaging system. This concept could also be applied to any other scanning pattern that unevenly samples the entire FOV during construction of a single frame,

0003-6935/11/162376-07$15.00/0

such as the rose or propeller scan. Similar methods have since been demonstrated in a high-speed miniaturized multiphoton microscope [5] and a handheld dual-axes confocal microscope [7].

This fast-updating image reconstruction method effectively subsamples a slower, more densely sampled Lissajous scanning pattern and quickly displays the partially scanned frames to provide imaging faster than the pattern repeat rate. Because the Lissajous pattern continuously scans across the entire FOV while completing one cycle of the Lissajous pattern, partially scanned frames contain sufficient information from throughout the FOV to reconstruct the image. Since the scanning pattern is not repeated in any two subsequent frames, pixels that are unsampled in one frame may be sampled in the next, which reduces the appearance of unsampled pixels to the user when viewed at higher frame rates. No pixel information is discarded compared to the traditional image reconstruction method, meaning that the traditional image can still be reconstructed from the fast-updating images. We present methods for real-time display of both the traditional Lissajous-scanned image and a moving average image alongside the higher frame rate images, which provide additional image detail.

2. Lissajous Image Reconstruction Methods

A. Conventional Lissajous Reconstruction

Steering a laser beam by two orthogonal sinusoids produces a Lissajous pattern, where the location (x,y) of the focused laser beam is given by the parametric equations

$$x(t) = \frac{1}{2}X[\sin(2\pi f_x t + \phi_x) + 1], \tag{1}$$

$$y(t) = \frac{1}{2}Y[\sin(2\pi f_y t + \phi_y) + 1]. \tag{2}$$

Here f and ϕ are the driving frequency and phase shift, respectively, in the x or y directions, and X and Y are the maximum extents of the FOV in x and y, respectively. For image reconstruction, Eqs. (1) and (2) describe the pixel location of each data sample where X and Y are in units of pixels. The pattern repeat rate, f_P, of a Lissajous pattern is given by

$$f_P = \frac{f_x}{n_x} = \frac{f_y}{n_y}, \tag{3}$$

where n_x and n_y are the smallest integer divisors that satisfy Eq. (3). Thus, for all real and rational scanning frequencies, the corresponding Lissajous pattern is stable and will repeat at a fixed rate. The integers n_x and n_y determine the number of cycles that occur in either the x or y direction, respectively, before the pattern repeats [2]. Larger values of n increase the number of lines scanned across the FOV during one completion of the Lissajous pattern.

Within the resonance bandwidth of the scanning device, the driving frequencies can be chosen to maximize the n values that satisfy Eq. (3), thereby increasing the line density of the image. From Eq. (3), it is clear that an increase in line density inherently reduces the pattern repeat rate. When the frame rate (f_F) is made equal to f_P, as is commonly done, there exists an intrinsic trade-off between sampling density and frame rate. Furthermore, because the Lissajous pattern is repeated once for each frame, regions of the image left unsampled by a sparse Lissajous pattern in one frame remain unsampled in subsequent frames, and this information is lost.

For illustration, Fig. 1 displays MATLAB simulations for single Lissajous-scanned frames where $f_F = f_P$ for several scanning frequency combinations and pixel numbers. In these examples, the driving frequencies are restricted to the resonant scanning peaks of the MEMS scanning mirror used in our recently developed 9.6 mm diameter microsurgery probe [8]: $f_x = 980$ Hz with an 18 Hz bandwidth (FWHM) and $f_y = 2260$ Hz with a 100 Hz bandwidth. For quantitative comparison, Fig. 2 plots the percent of pixels sampled at least once and the percent of pixels sampled ten times or more for each integer frame rate achievable within these resonant bandwidths up to 35 frames per second.

In Fig. 1, pixels that do not get sampled by the Lissajous pattern are shown white. To reduce these unsampled pixels, higher line densities, and subsequently lower frame rates, can be used, and/or the relative pixel size can be increased. In either solution, pixels toward the outside of the image can be

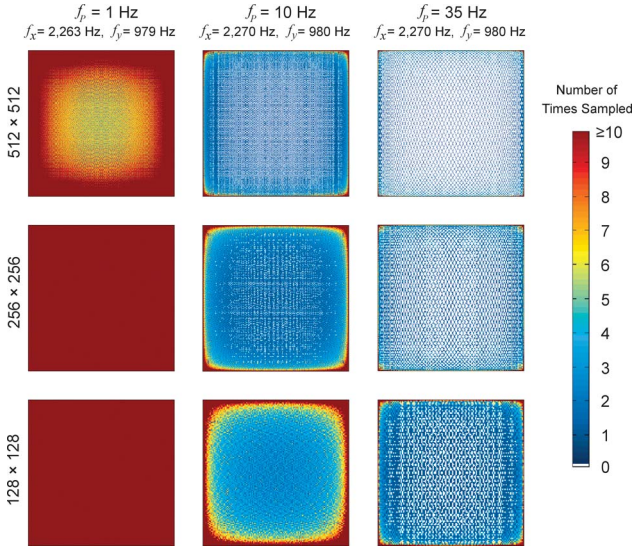

Fig. 1. (Color online) Conventional Lissajous reconstructions for various pattern repeat rates and pixel sizes. The color map represents the number of times a given pixel is sampled before one cycle of the Lissajous pattern completes. For the conventional case where $f_F = f_P$, this represents the number of times a pixel is sampled in each frame. White pixels denote unsampled regions of the image. Data generated by MATLAB simulation.

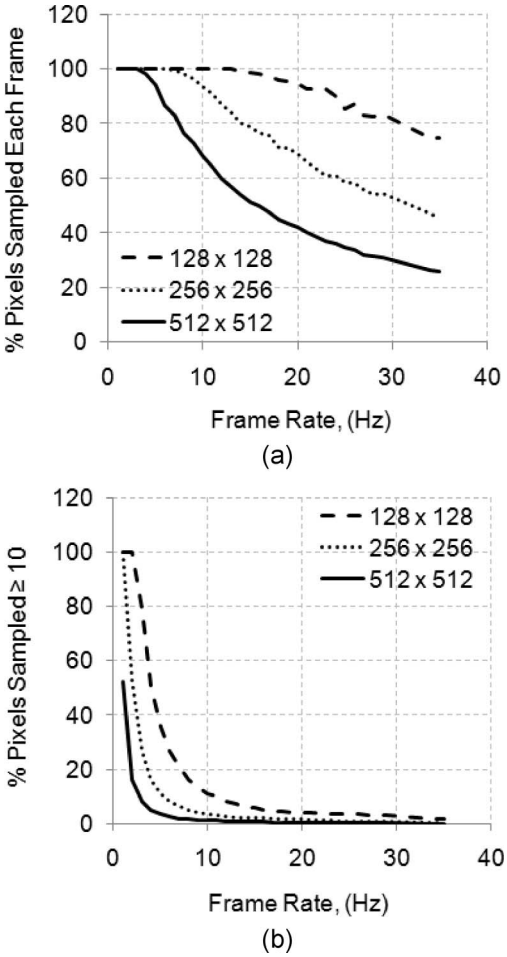

Fig. 2. Sampling statistics for conventionally reconstructed Lissajous images with resonant frequencies at $f_x = 2260\,\text{Hz}$ and $f_y = 980\,\text{Hz}$. (a) Percentage of pixels in each frame sampled for a given frame rate. (b) Percentage of pixels sampled ten times or more in each frame at a given frame rate. The solid, dotted, and dashed curves represent 512×512, 256×256, and 128×128 pixel images, respectively. Data generated by MATLAB simulation.

heavily oversampled (e.g., sampled ten or more times) in each frame. Moderate resampling of pixels can be useful in reducing noise if intensity values from different cycles within the same frame are averaged; however, significant resampling of pixels provides little new spatial information despite the increased laser exposure to these oversampled regions.

When selecting the number of pixels for a given FOV, we need to consider several constraints. On one hand, as seen in Figs. 1 and 2, image reconstruction with a fewer number of pixels can reduce the number of unsampled pixels to achieve a completely filled image. On the other hand, for a given FOV and resolution, there is a minimum number of pixels that can be used before the image resolution becomes limited by the pixel size. Using the Nyquist criterion, we desire at least two pixels per resolvable spot in our image. Thus, for an example case of a $200\,\mu\text{m} \times 200\,\mu\text{m}$ FOV and a $1\,\mu\text{m}$ resolution, this criteria requires the reconstructed image consist of no fewer than $400\,\text{pixels} \times 400\,\text{pixels}$. However, in addition to increasing the likelihood of unsampled pixels, increasing the number of pixels used in image reconstruction also increases the required data acquisition rate to avoid missing pixels at the center of the image. Explicitly, the pixel scanning speed can be expressed by the first derivatives of Eqs. (1) and (2):

$$\dot{x}(t) = \pi f_x X[\cos(2\pi f_x t + \phi_x)], \tag{4}$$

$$\dot{y}(t) = \pi f_y Y[\cos(2\pi f_y t + \phi_y)]. \tag{5}$$

When both axes are traveling at their maximum velocity, which occurs at the center of the image, the maximum scanning speed, $v_{\max}$, in pixels per second is given by

$$v_{\max} = \pi P\sqrt{f_x^2 + f_y^2}, \tag{6}$$

for a square image in which $X = Y = P$. In the example case where $P = 400$, $f_x \approx 980\,\text{Hz}$, and $f_y \approx 2260\,\text{Hz}$, $v_{\max} = 3.1 \times 10^6$ pixels/s. Therefore, the data acquisition rate must equal or exceed 3.1 MHz to avoid missing pixels in the center of the image, and thus the image size introduces hardware constraints in addition to resolution constraints.

As illustrated in Figs. 1 and 2, it is possible to completely fill images with large numbers of pixels by selecting driving frequencies corresponding to a slowly repeating Lissajous pattern. However, for use in a clinical imaging system, slow frame rates lead to motion artifacts, while large oversampling leads to unnecessarily high laser dosages. While the 10 Hz updating pattern with a 256 pixel × 256 pixel image size appears to be a good compromise in our example, approximately 6.5% of the pixels toward the center of the image remain unsampled and will be unsampled in every frame, resulting in a small loss of information. What we desire is to achieve full coverage of the FOV, such as the one found with the 1 Hz updating pattern, but with the ability to capture dynamic information at a faster rate and to use the laser exposure more efficiently.

B. Fast-Updating and Nonrepeating Lissajous Reconstruction

To improve upon this traditional approach to Lissajous image reconstruction for clinical imaging applications, we have implemented a new fast-updating Lissajous image reconstruction method where the Lissajous pattern does not repeat for each frame. In this method, we drive the scanning device at resonant frequencies that can provide a high line density but update the frame at a rate many times faster than the pattern repeat rate. Here we simply take advantage of the fact that a Lissajous scanning pattern repeatedly samples across the entire extent of the FOV while acquiring information for a given frame. Thus, information about the entire FOV can be extracted from a partially scanned frame.

In our method, the image reconstruction algorithm tracks the pixel location continuously over time, rather than refreshing at the end of each frame. The location for the first pixel of each frame is dictated by the Lissajous trajectory and pixel location at the end of the preceding frame. The frame rate, f_F, is then set independently of f_P to optimize single-frame detail and imaging speed ($f_F > f_P$). In this manner, the number of oversampled pixels in a single frame is greatly reduced, and the frame rate is increased for increased temporal resolution. Figure 3 compares the percent of pixels sampled once and sampled ten or more times using this method using a 1 Hz Lissajous pattern ($f_x = 979$ Hz and $f_y = 2263$ Hz) for frame rates from 1 to 10 frames/s and 512 pixel × 512 pixel image reconstruction. Using this method, the scanning pattern for each frame is distinct until the 1 Hz Lissajous pattern begins to repeat. In other words, a 5 Hz frame rate will consist of a repeating series of five distinct frames. In Fig. 3, the statistics for each distinct frame are provided to show frame-to-frame variability.

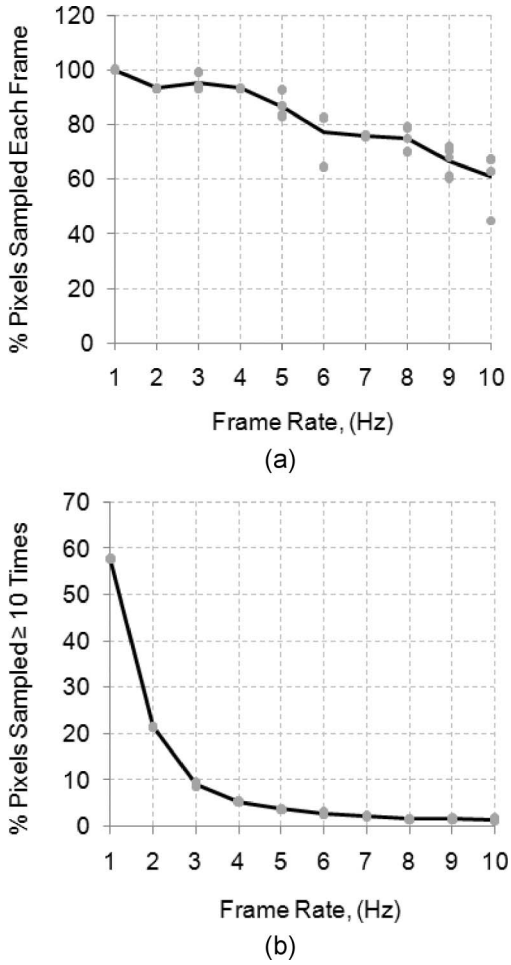

Fig. 3. Sampling statistics for Lissajous images reconstructed using our fast-updating method with scanning frequencies of $f_x = 2260$ Hz and $f_y = 979$ Hz and a 512 × 512 image size. (a) Percentage of pixels in each frame sampled for a given frame rate. (b) Percentage of pixels sampled ten times or more in each frame at a given frame rate. The gray circles denote the values for each frame at a given frame rate, while the solid line displays the average for each frame rate. Data generated by MATLAB simulation.

From Fig. 3 we see that the percentage of pixels sampled per frame in our method decreases with increasing frame rate at a similar rate to the conventional reconstruction where $f_F = f_P$. However, in our method the pixels that are unsampled in a given frame are generally sampled in the subsequent frame, since the pattern does not repeat for each frame. Furthermore, due to the increased frame rate, the overall sampled pixel density can appear higher as the frame rate approaches the flicker fusion threshold of the human visual response [9]. Critically, *no information is lost from the conventional slower-displaying Lissajous image*. The information is simply separated and displayed into shorter time intervals to capture additional dynamic information. Thus, both the fast-updating, lower-pixel density image of our fast-updating algorithm and the slower, high-pixel density image of the traditional algorithm can be viewed side-by-side during real-time image reconstruction.

3. Experimental Implementation

We first incorporated the image reconstruction methodology described above into the miniaturized 18 mm probe we have designed for combined nonlinear optical microscopy and femtosecond laser microsurgery [4]. Here we will present results from the most recent 9.6 mm diameter probe [8]. This new smaller probe utilizes a two-axis resonant MEMS scanning mirror with the resonant frequencies described earlier. We drive the mirror at $f_x = 979$ Hz and $f_y = 2263$ Hz, and reconstruct and display 512 pixel × 512 pixel frames at a frame rate of 7 Hz. These scanning patterns correspond to the 1 Hz pattern shown in Fig. 1. Based on the measured 1.32 μm two-photon resolution of our 9.6 mm probe, this pattern can provide full coverage at the sample for FOV well over 1 mm × 1 mm. Based on Fig. 3, reconstruction at 7 frames/s is an attractive choice, as it offers a 7× enhancement in temporal resolution over the conventional reconstruction method, which updates at 1 Hz for these scanning frequencies. Also, at 7 Hz reconstruction, each frame samples approximately the same number of pixels (>76%) with little visible frame-to-frame variability.

A custom LabVIEW program implements our image reconstruction algorithm, shown in Fig. 4. The program drives the scanning mirror and handles real-time image reconstruction and display through two data acquisition cards. One high-speed analog input card (PCI-6115, National Instruments) is used for collecting the image data and to drive one axis of the MEMS mirror. The other card (PCI-6711, National Instruments) is used to drive the second axis of the MEMS mirror. We used the second card to provide additional analog output channels, because we were limited by the output channels available on our data acquisition card. The two cards are connected with a real-time system integration

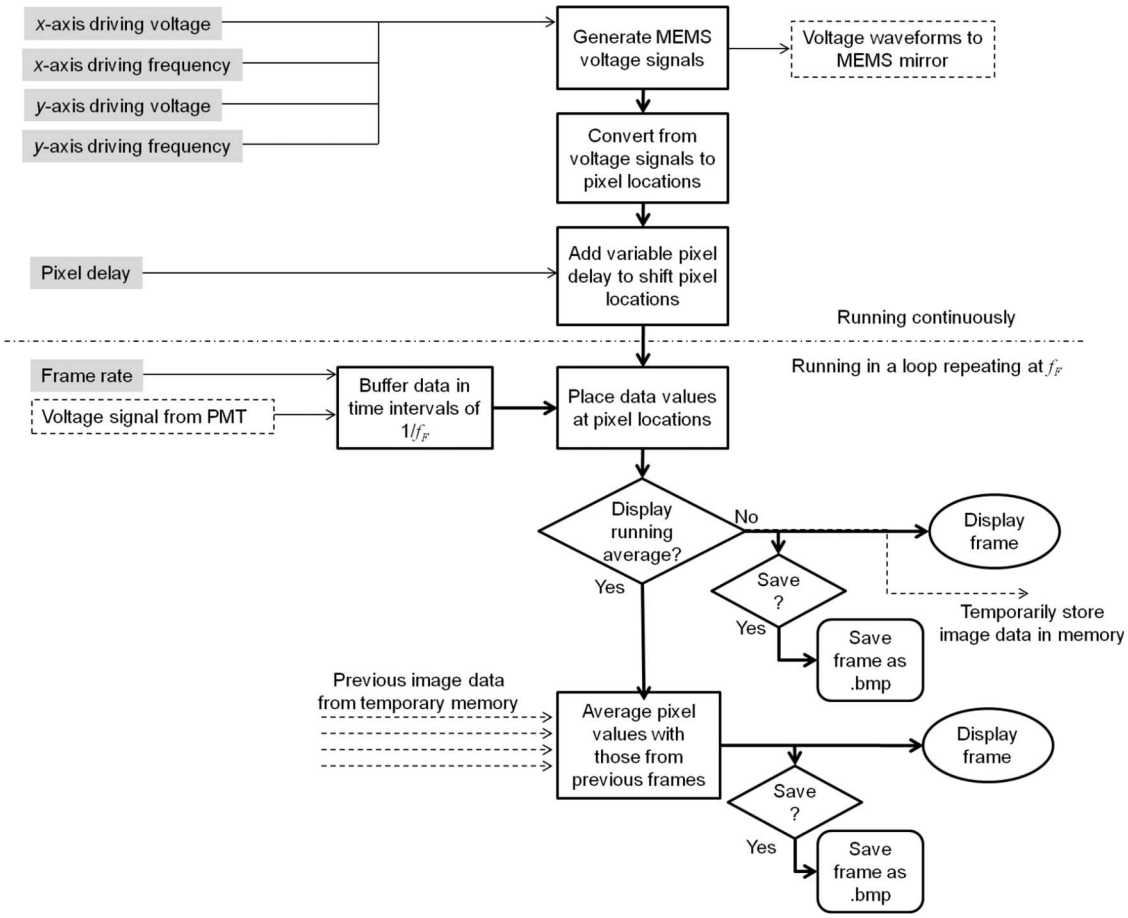

Fig. 4. Flow chart illustrating our fast-updating Lissajous image reconstruction algorithm. User inputs are shaded gray and located on the left. User-selectable options are denoted by diamond process blocks. The MEMS driving signal and the data collection are synchronized by triggering from the same master clock in the software and by linking the data acquisition cards physically with a RTSI cable.

(RTSI) cable to allow synchronization to a common clock.

For nonlinear optical imaging, we digitize the photocurrent from a photomultiplier tube (PMT) (H7422-40, Hamamatsu) at a sampling rate of 4 MHz through a high-speed preamplifier (DHPCA-100, FEMTO Messtechnik). This sampling rate allows reconstruction of up to 512 pixel × 512 pixel images at the given scanning frequencies without missed pixels at the center of the FOV arising from the high scanning speed. The collected data are stored in the memory buffer until it is time to display the next frame, as determined by the frame rate.

The sinusoidal driving waveforms to the MEMS mirror are generated according to the frequencies and peak voltage values defined by the user. By varying the peak driving voltage, we can adjust the amplitude of mirror deflection and thus control the magnification of the microscope. For proper synchronization, the sampling rate for the generated waveforms must be equal to the input sampling rate, which is 4 MHz in our case. The program next digitizes the driving voltage waveforms into pixel locations for image reconstruction. We have implemented a real-time variable phase delay control, which allows us to shift the pixel locations along the Lissajous trajectory to compensate for phase delay between mirror driving signal and pixel location. The resulting array of pixel coordinates is buffered until all image data have been collected for the current frame, at which point the image data are placed in a 512×512 array according to the corresponding pixel location coordinates and displayed as an image.

For pixels that are sampled multiple times in a single frame, the most recent value is used, rather than averaging the values. While averaging can help suppress noise, selective pixel-by-pixel averaging during image reconstruction was found to be too computationally intensive.

Proper synchronization is maintained in the program by triggering data collection and waveform generation off the hardware clock. The clocks of the two cards are synchronized via the RTSI cable. Maintaining proper synchronization is critical to this technique, as temporal drift may lead to accumulating artifacts in the image. We have implemented our image reconstruction program on a personal computer with a 2.8 GHz quad-core Intel i7-860 processor and 3.5 GB of random access memory (RAM) running LabVIEW 2009 on the Windows XP Professional operating system. With the current hardware and LabVIEW code, our fast-updating Lissajous image

reconstruction algorithm is capable of displaying frame rates up to 15 Hz without loss of data or departure from the desired frame rate. We believe this speed could be increased through further optimization of the code; however, frames taken at such high speeds will sample only a small percentage of pixels per frame.

The program can display in three different image construction modes: (1) the conventional Lissajous image at 1 Hz, (2) our fast-updating Lissajous image at 7 Hz, or (3) a third imaging mode, called "moving average," in which we average every 7 Hz image with the six previous images. The moving average image provides all the detail of the 1 Hz image, along with noise suppression from averaging, at the cost of introducing mild motion artifacts. By averaging entire frames, we can achieve real-time noise suppression in a computationally efficient manner.

Figure 5 shows an image acquired using our fast-updating Lissajous scanning algorithm [Fig. 5(a)], a moving average image [Fig. 5(b)], along with a frame acquired at 1 Hz showing the traditional Lissajous scanning algorithm [Fig. 5(c)]. As seen in Fig. 5(a), the frame updating at 7 Hz with the fast-updating Lissajous image reconstruction algorithm provides information from the entire FOV; however, the FOV is only sparsely sampled compared to the conventional Lissajous pattern shown in Fig. 5(c). Note that, because the optical focusing conditions at the sample remain unchanged across all reconstruction methods, the resolution is unaffected in Figs. 5(a)–5(c) although the image is more sparsely sampled in Fig. 5(a). On the other hand, the frame in Fig. 5(a)

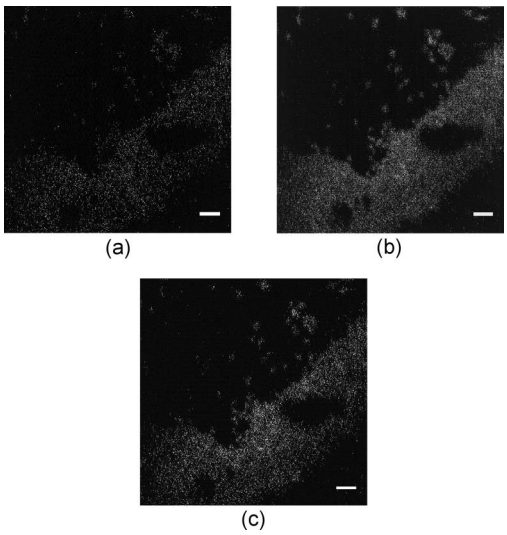

Fig. 5. Two-photon fluorescence images of 1 μm fluorescent beads deposited on glass. (a) Raw frame using the fast-updating image reconstruction algorithm updating at 7 Hz. (b) Frame taken using the moving average algorithm, averaging seven raw frames and updating at 7 Hz. (c) Frame taken using the conventional Lissajous image reconstruction methodology, updating at the pattern repeat rate of 1 Hz. Contrast has been increased on the moving average image to match that of the unaveraged images. Scale bars are 10 μm.

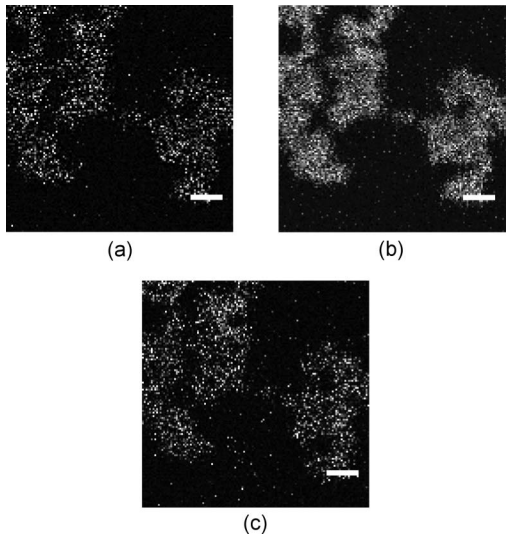

Fig. 6. Images from real-time videos (Media 1, Media 2, Media 3) of 1 μm fluorescent beads dried on a glass microscope slide and translated manually at varying speeds. The videos demonstrate the effect of each image reconstruction algorithm. (a) Our fast-updating algorithm updating at 7 Hz. (b) Moving average algorithm updating at 7 Hz displaying a seven frame moving average. (c) Conventional 1 Hz image reconstruction. Note that the conventional algorithm video contains motion artifacts not present in the fast-updating algorithm video. The image reconstruction size was reduced here to 128 pixels × 128 pixels to demonstrate the denser sampling that can be achieved with small FOV. Contrast has been adjusted on the moving average image to match that of the unaveraged images. Scale bars are 5 μm.

contains the desired fast dynamic information because the frames refresh seven times faster. This aspect can only be truly appreciated when viewing the frames streaming at their respective rates, and Media 1, Media 2, and Media 3 show video taken using our 7 Hz frame rate fast-updating algorithm, the moving average algorithm, and finally the traditional algorithm.

In Fig. 6(a), the movement of the beads can be followed easily with little or no noticeable motion artifacts, depending on the speed. While the percent of pixels sampled in each individual frame in Fig. 6(a) is reduced compared to the traditional Lissajous image in Fig. 6(c), individual beads can still clearly be distinguished and show no change in fundamental resolution (i.e., the size of a single bead). Use of the moving average algorithm in Fig. 6(b) provides superior detail over the traditional image due to the noise reduction arising from averaging, though at the cost of the introduction of motion artifacts compared to the raw 7 Hz images. Because the moving average images still update at 7 Hz, however, the user is still able to identify and react to the occurrence of fast dynamic events faster than in the traditional 1 Hz image.

4. Conclusion

We have presented a simple fast-updating image reconstruction algorithm for use with Lissajous-scanned imaging systems. This modification is

particularly useful in resonantly scanned laser microscopy systems, wherein the choice of scanning frequencies is restricted to the bandwidth of the resonant peaks. Our method provides an alternative to using the pattern repeat rate as the frame rate, thus enabling dynamic visualization of samples with higher temporal resolution. This method is simple to implement and results in no loss in information from the conventional Lissajous-scanned image, as the conventional image can be displayed simultaneously. Using our method, the trade-off between single-frame pixel density and frame rate can be chosen freely by the user, whereas only a limited number of practical options may be available using the conventional method with narrow-bandwidth resonant scanning devices. In addition to the miniaturized multiphoton imaging system shown here, this fast-updating image reconstruction algorithm can be broadly applied for any Lissajous-based laser scanning imaging system in which greater temporal resolution is desired.

The authors acknowledge support from the National Science Foundation under grants BES-0548673, CBET-1014953, and Career Award CBET-0846868 as well as a grant from the Texas Ignition Fund by the University of Texas Board of Regents. Also, the authors would like to thank Olav Solgaard for supplying the MEMS scanning mirror used in the miniaturized microscope and Pengyuan Chen for LabVIEW assistance.

References

1. D. L. Dickensheets and G. S. Kino, "Micromachined scanning confocal optical microscope," Opt. Lett. **21**, 764–766 (1996).
2. F. Helmchen, M. S. Fee, D. W. Tank, and W. Denk, "A miniature head-mounted two-photon microscope: high-resolution brain imaging in freely moving animals," Neuron **31**, 903–912 (2001).
3. B. A. Flusberg, J. C. Jung, E. D. Cocker, E. P. Anderson, and M. J. Schnitzer, "*In vivo* brain imaging using a portable 3.9 gram two-photon fluorescence microendoscope," Opt. Lett. **30**, 2272–2274 (2005).
4. C. L. Hoy, N. J. Durr, P. Chen, W. Piyawattanametha, H. Ra, O. Solgaard, and A. Ben-Yakar, "Miniaturized probe for femtosecond laser microsurgery and two-photon imaging," Opt. Express **16**, 9996–10005 (2008).
5. T.-M. Liu, M.-C. Chan, I. H. Chen, S.-H. Chia, and C.-K. Sun, "Miniaturized multiphoton microscope with a 24 Hz frame-rate," Opt. Express **16**, 10501–10506 (2008).
6. J. A. Lissajous, "Note sur un nouveau moyen de mettre en évidence le mouvement vibratoire des corps," C. R. Hebd. Seances Acad. Sci. **41**, 93–95 (1855).
7. J. T. C. Liu, M. J. Mandella, N. O. Loewke, H. Haeberle, H. Ra, W. Piyawattanametha, O. Solgaard, G. S. Kino, and C. H. Contag, "Micromirror-scanned dual-axis confocal microscope utilizing a gradient-index relay lens for image guidance during brain surgery," J. Biomed. Opt. **15**, 026029 (2010).
8. C. L. Hoy, W. Piyawattabanetha, H. Ra, O. Solgaard, and A. Ben-Yakar, "Optical design and imaging performance testing of a 9.6 mm diameter femtosecond laser microsurgery probe," Opt. Express **19**, 10536–10552 (2011).
9. C. Landis, "Determinants of the critical flicker-fusion threshold," Physiol. Rev. **34**, 259–286 (1954).